

引用格式：冯杭建，邱尔康，金宠，等，2025. 浙东南火山岩区磷灰石裂变径迹研究及地质意义[J]. 地质力学学报, 31(4): 589–603.
DOI: [10.12090/j.issn.1006-6616.2025016](https://doi.org/10.12090/j.issn.1006-6616.2025016)

Citation: FENG H J, QIU E K, JIN C, et al., 2025. Apatite fission-track study of the volcanic rock area in southeast Zhejiang Province and its geological significance[J]. Journal of Geomechanics, 31(4): 589–603. DOI: [10.12090/j.issn.1006-6616.2025016](https://doi.org/10.12090/j.issn.1006-6616.2025016)

浙东南火山岩区磷灰石裂变径迹研究及地质意义

冯杭建，邱尔康，金宠，林丹，徐兴华，蔡遥

FENG Hangjian, QIU Erkang, JIN Chong, LIN Dan, XU Xinghua, CAI Yao

浙江省地质院，杭州浙江 310007

Zhejiang Institute of Geosciences, Hangzhou 310007, Zhejiang, China

Apatite fission-track study of the volcanic rock area in southeast Zhejiang Province and its geological significance

Abstract: [Objective] As an essential component of the East Asian continental margin, the southeastern coastal region of China records a complex history of regional tectonics, magmatism, and geomorphological features associated with the subduction of the Paleo-Pacific/Pacific Plate. This region serves as an ideal window for studying ocean-continent interactions related to subduction zones. During the Cretaceous period, influenced by the rollback of the Paleo-Pacific Plate, a giant rhyolitic volcanic belt approximately 1200 km in length developed along the southeastern coast of China. Among the provinces in this region, Zhejiang hosts the largest preserved area of rhyolitic volcanic rocks and retains the most well-preserved volcanic structures. Previous studies have extensively investigated the geochronology, petrology, geochemistry, and metallogenesis of these rhyolitic volcanic rocks; however, their uplift and cooling history has been largely overlooked. [Methods] This study conducted apatite fission track dating and HeFTy thermal history modeling on the central facies intrusive rocks (quartz syenite, syenite and monzonite) of the calderas in the Yandang Mountain and Shenxianju areas. [Results] All the apatite fission track dates from the Yandang Mountain and Shenxianju areas show chi-squared probability $P(\chi^2) \geq 0.05$, indicating that the fission track dates of all specimens follow a Poisson distribution and belong to a single age population. Twenty of the total thirty-two specimens from the Yandang Mountain area yielded apatite fission track ages (pooled age and central age) between 40 Ma and 31 Ma, seven of the thirty-two specimens gave apatite fission track ages between 50 Ma to 41 Ma, with only five of the thirty-two specimens yielding apatite fission track ages ranging from 61 Ma to 51 Ma. For the Shenxianju area, the apatite fission track ages are predominantly (sixteen of the twenty-six specimens) distributed between 40 Ma and 31 Ma, with some specimens (eight of the twenty-six specimens) showing ages ranging from 50 Ma to 41 Ma and a few of them (two of the twenty-six specimens) yielding ages between 61 Ma and 51 Ma. Furthermore, the single-grain apatite fission track ages of the specimens from both the Yandang Mountain and Shenxianju areas show a unimodal distribution with a peak at 33 Ma. The mean confined track lengths of the specimens from the Yandang Mountain area vary between $\sim 11.12 \mu\text{m}$ and $\sim 14.09 \mu\text{m}$ with unimodal track length distributions. Specimens from the Shenxianju area yielded mean confined track lengths of ~ 11.11 to $\sim 14.44 \mu\text{m}$, also showing a unimodal track length distribution pattern. The mean D_{par} values of specimens from the Yandang Mountain area range from $0.78 \mu\text{m}$ to $1.04 \mu\text{m}$, while those from the Shenxianju area display mean D_{par} values varying from $0.86 \mu\text{m}$ to $1.12 \mu\text{m}$. The HeFTy thermal history modeling reveals a rapid exhumation and cooling event occurring from the early-

基金项目：浙江省级基础性公益性战略性地质工作项目资金（省资〔2015006〕，〔省资〕2023017，〔省资〕2025009）；国家自然科学基金项目（42277132）

This research is financially supported by the Zhejiang Provincial Funds for Fundamental, Public-Welfare and Strategic Geological Projects (Grant Nos. 2015006, 2023017 and 2025009) and the National Natural Science Foundation of China (Grant No. 42277132).

第一作者：冯杭建（1979—），男，博士，高级工程师，主要从事地质遗产保护与地貌学方面研究。Email: Pcerma@foxmail.com

收稿日期：2025-02-28；修回日期：2025-05-27；录用日期：2025-06-30；网络出版日期：2025-06-30；责任编辑：王婧

Eocene to the earliest Oligocene for both the Yangdang Mountain (48 Ma to 33 Ma) and Shenxianju (52 Ma to 32 Ma) areas. The cooling rates of this event vary from ca. 8 °C/Myr to 20 °C/Myr for Yandang Mountain area and ca. 5 °C/Myr to 16 °C/Myr for Shenxianju area respectively. [Conclusion] Our new apatite fission track dating and HeFTy thermal history modeling results help identify an exhumation and cooling event in the Yangdang Mountain and Shenxianju areas during the early-Eocene to the earliest Oligocene epoch. Based on the results of this study and regional tectonic setting analysis, the early-Eocene to the earliest Oligocene exhumation and cooling event in the study areas is interpreted as being initially controlled by the subduction of the Izanagi-Pacific Plate ridge and later driven by the combined effects of the India-Eurasia continental collision and the rollback of the Pacific Plate. [Significance] This study provides important low-temperature thermal geochronological constraints on the Phanerozoic regional tectonic and geomorphological evolution of southeastern Zhejiang province.

Keywords: apatite fission track; Yandang Mountain; Shenxianju; Cretaceous volcanic rock ; subduction of Pacific slab; chronology

摘要: 中国东南沿海诸省发育了一条长约 1200 km 的巨型流纹质火山岩带，其中浙江是流纹质火山岩保存面积最大、各类型火山岩构造最完好的省份。目前，浙江省流纹质火山岩的年代学、岩石学、地球化学及矿床学特征已有大量研究，但其后期的抬升剥露历史缺乏系统约束。文章以浙江省东南部雁荡山与神仙居 2 处复活破火山为研究对象，对其中心相侵入岩开展磷灰石裂变径迹年代学分析与 HeFTy 热史模拟。结果表明，浙江省东南部雁荡山与神仙居中心相侵入岩的磷灰石裂变径迹年龄多数集中于 40~31 Ma，且峰值为 33 Ma，部分分布于 50~41 Ma，仅少量分布于 61~51 Ma；热史模拟结果显示，雁荡山与神仙居地区在始新世早期（约 52~48 Ma）至渐新世最早期（34~32 Ma）经历了 1 期快速抬升冷却事件，该抬升冷却事件早期受控于伊泽那崎-太平洋板块洋脊的俯冲，晚期则由印度-欧亚大陆碰撞汇聚的远程效应与太平洋板块俯冲后撤的共同驱动。研究结果可为浙东南地区新生代大地构造和区域地貌演化提供重要的低温热年代学约束。

关键词：磷灰石裂变径迹；雁荡山；神仙居；白垩纪火山岩；太平洋俯冲；年代学

中图分类号：P548; P56 **文献标识码：**A **文章编号：**1006-6616(2025)04-0589-15

DOI: [10.12090/j.issn.1006-6616.2025016](https://doi.org/10.12090/j.issn.1006-6616.2025016)

0 引言

东亚大陆边缘自晚三叠世—早侏罗世时期起开始接受古太平洋板片的俯冲作用，形成主动大陆边缘并延续至今(Li and Li, 2007; Müller et al., 2016; Li et al., 2019)。作为东亚大陆边缘的重要组成部分，中国东南沿海地区记录了多期由古太平洋-太平洋板片俯冲导致的地壳变形、岩浆活动及区域变质事件(Li et al., 2014; Suo et al., 2020; Xu et al., 2023)，是研究洋-陆俯冲及主动大陆边缘演化的理想对象。白垩纪时期，古太平洋板片俯冲发生后撤，导致华南岩石圈发生大规模伸展减薄、岩石圈拆沉及其下伏软流圈的上涌(Xu et al., 2021; Li et al., 2022a; Dong et al., 2023)，产生了强烈的岩浆活动(Lapierre et al., 1997; Zhou et al., 2006)，在中国东南沿海浙、苏、皖、闽、赣、粤、琼诸省形成了一条长约 1200 km、呈北东走向的巨型中生代流纹质火山

岩带(Zhou and Li, 2000; Xu et al., 2021)，其中浙江的流纹质火山岩具有典型性和代表性。

学者们对浙江省白垩纪流纹质火山岩开展了大量研究，并取得了一系列成果，基本厘定了浙江省流纹质火山岩的喷发期次与地层年代学格架(俞云文和徐步台, 1999; Liu et al., 2014; 浙江省地质调查院, 2024)、岩石成因与岩浆作用过程(段政等, 2015; Yan et al., 2016; Zhang et al., 2018; Li et al., 2022b)，并在与之相关的成矿作用上取得了一定突破(周乐尧等, 2013; Fang et al., 2020; Zhou et al., 2021, 2022)。然而，已有研究很少涉及浙江白垩纪流纹质火山岩及与之相关的侵入岩体形成后的埋藏-抬升-剥露历史，制约了对该地区晚白垩世以来大地构造、地貌演化及相关矿床保存情况的认识。基于此，文章以浙江东南部雁荡山及神仙居地区为研究区，开展磷灰石裂变径迹研究，以期探寻其抬升-冷却历史并探讨相关的大地构造背景。

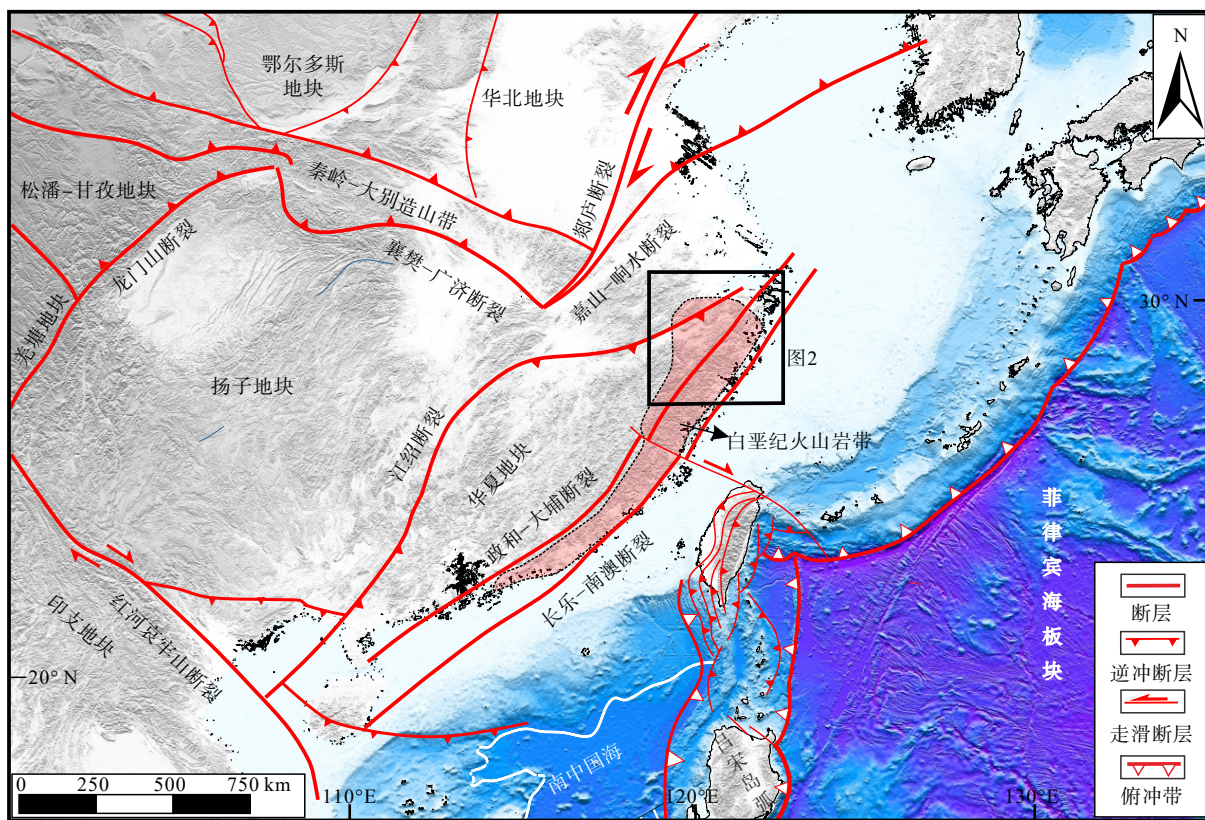


图 1 中国东南海沿海及其周边地区大地构造简图(据李三忠等, 2018 修改)

Fig. 1 Sketched tectonic map of southeastern coastal area of China and its adjacent areas (modified after Li et al., 2018)

1 区域地质背景与采样

1.1 区域地质背景

浙江省位于华南板块的东部, 以江山-绍兴断裂为界, 西北部地区属于扬子地块, 东南部属于华夏地块(水涛等, 1986; 水涛, 1987; Zheng et al., 2013)。作为中国东南沿海白垩纪巨型火山岩带的重要组成部分(图 1), 浙江省内白垩纪流纹质火山岩分布面积达 41000 km²。

浙江白垩纪酸性火山岩带分布数个大型环状火山构造/机构(图 2), 浙江东南部括苍山巨型环状火山构造及其东南侧的雁荡山为其中典型代表(阮宏宏等, 1988; 张福祥和张登荣, 1990)。括苍山巨型环状火山构造北起天台、南至永嘉(位置见图 2 绿色虚线), 内部包含有多个破火山口、火山穹窿与火山沉积洼地, 位于西南部的神仙居为其中保存较好的破火山口(阮宏宏等, 1988, 1993)。既往研究将括苍山-雁荡山地区的火山活动划分为 4 个火山旋回(谢家莹和徐忠连, 1988): 火山喷发-侵入穹窿(I)、破火山口(II)、上叠式火山沉积洼地和破火山口

(III)以及锥火山和小型破火山口(IV)。其中 I、II 旋回酸性火山岩主要岩性为凝灰熔岩、多晶屑熔结凝灰岩、凝灰岩与火山灰流凝灰岩, 相当于下火山岩系的高坞组-西山头组(阮宏宏等, 1988; 王学颖等, 2023); 而 III、IV 旋回岩性变化大、并与沉积碎屑岩层交互产出, 相当于上火山岩系的馆头-塘上组(阮宏宏等, 1988, 1993)。

雁荡山为典型的白垩纪复活型破火山, 其形成经历了 4 期火山喷发和 1 期侵入作用, 其喷出岩自下而上主要岩性分别为低硅熔结凝灰岩、流纹岩、凝灰岩和熔结凝灰岩(陶奎元等, 2004)。锆石 U-Pb 年代学揭示该地区的 4 期火山作用时限在 105~97 Ma(余明刚等, 2006), 而中心侵入相石英正长斑岩的形成年龄为 98±1 Ma (He et al., 2009)。现有系统性的岩石学与地球化学研究表明, 雁荡山火山岩代表了该期岩浆活动过程中的高分异端元, 而中心侵入相石英正长斑岩为浅部岩浆房中的残留晶粥(Yan et al., 2016), 二者在成因上互相联系。神仙居同样为白垩纪复活型破火山, 其形成经历了 2 期火山-沉积旋回, 下部为火山碎屑岩及流纹岩, 上部为流纹岩、球泡流纹岩、含晶屑玻屑熔结凝灰岩与流

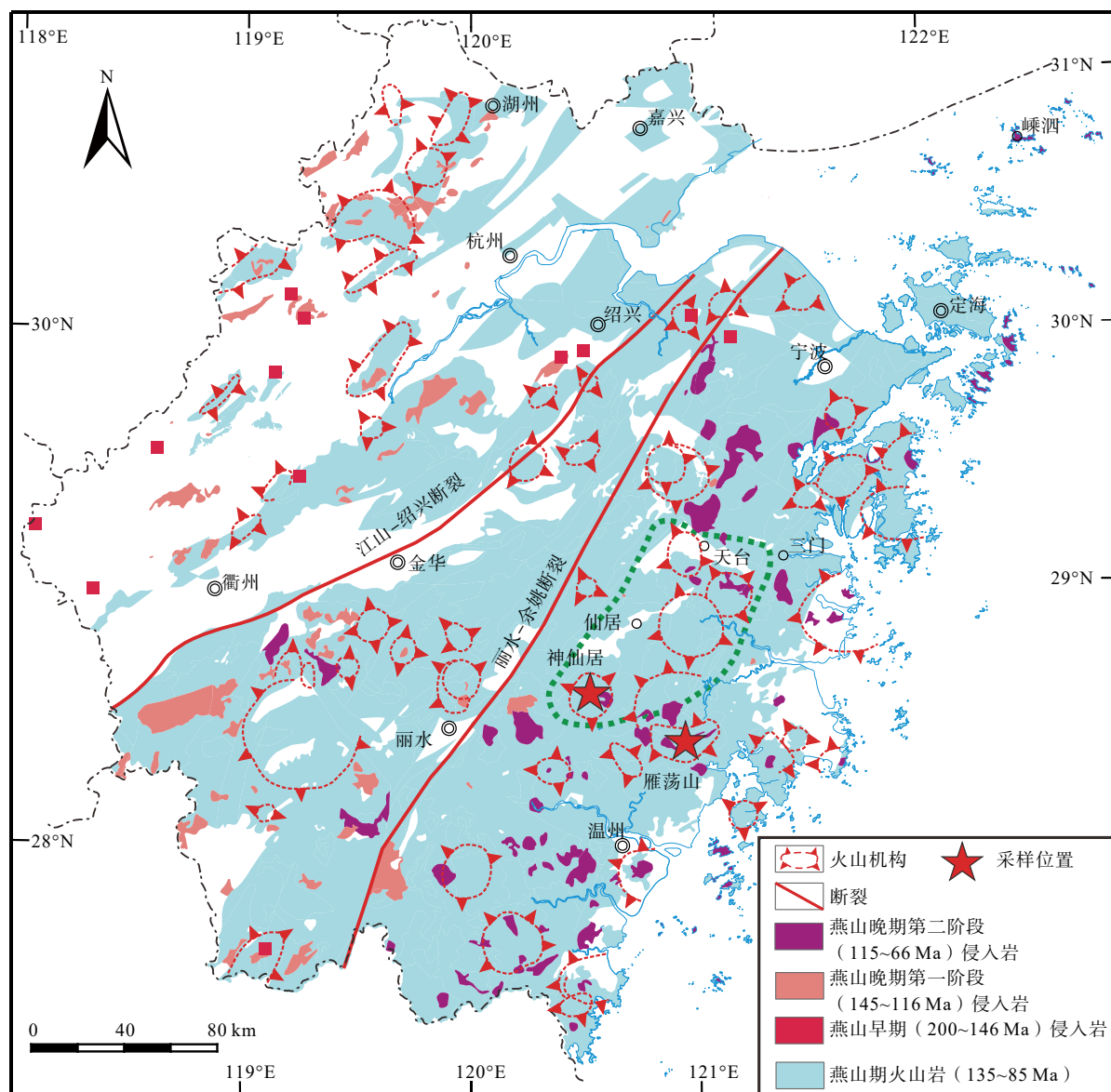


图 2 浙江省燕山期岩浆岩分布图 (绿色虚线为括苍山巨型环状火山构造; 浙江省燕山早期侵入体面积均过小, 故在图中以红色方框标注其所在位置)

Fig. 2 Distribution map of Yanshanian magmatic rocks in Zhejiang Province (The green dashed line represents the Kuocangshan circular volcanic edifice; The locations of early Yanshanian intrusions in Zhejiang province are marked by red squares.)

纹质熔结凝灰岩。锆石 U-Pb 年代学测试结果表明其上部流纹质熔结凝灰岩形成时代约为 114~113 Ma(唐增才等, 2018)。

1.2 采样描述

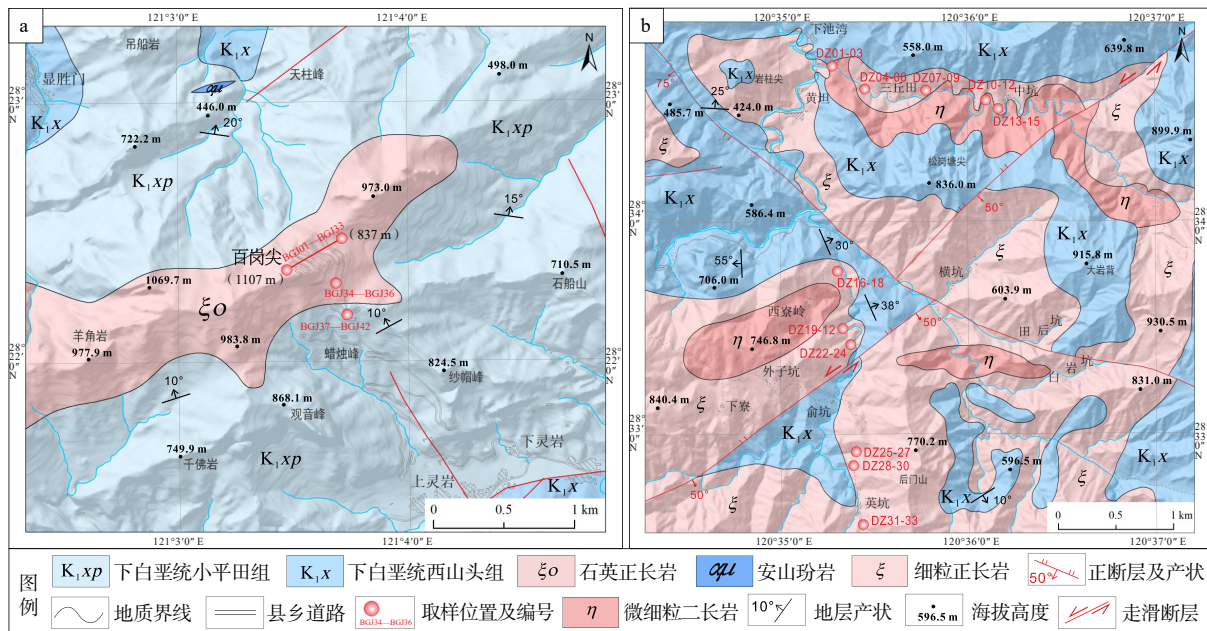
此次研究对雁荡山百岗尖地区和神仙居淡竹地区出露的火山机构中心相侵入岩体进行采集, 用于磷灰石裂变径迹分析, 以期获得 2 个地区较为完整的冷却抬升历史。其中雁荡山百岗尖地区采集样品岩性均为石英正长岩, 神仙居淡竹地区采集样品岩性为微细粒二长岩与细粒正长岩; 雁荡山百岗尖地区取样高程从 250 m 至 1107 m, 神仙居仙居淡

竹地区取样高程从 252 m 至 522 m, 垂直高程每间隔 10~20 m, 具体采样位置见图 3。在雁荡山百岗尖地区取样 32 件, 在神仙居淡竹地区取样 26 件, 共 58 件样品, 具体采样信息见表 1。

2 磷灰石裂变径迹测试与热史模拟方法

2.1 磷灰石裂变径迹测试方法

岩石样品的碎样与磷灰石颗粒的挑选工作由化工地质矿山第十八实验室和廊坊市诚信地质服务有限公司完成。首先通过传统的粉碎机碎样、标



a—雁荡山地区采样位置图(BGJ01—BGJ33样品沿图中标注取样剖面线位置等间距取样); b—神仙居地区采样位置图

图3 磷灰石裂变径迹分析采样位置图

Fig. 3 Sample location maps for apatite fission track analysis in Zhejiang Province

(a) Sample location in the Yandangshan area (Sample BGJ01 to BGJ33 were sampled at equal intervals along the section marked in the figure);
 (b) Sample location in the Shenxianju area

准重液及磁分选方法分离出样品中的磷灰石颗粒;随后,在双目显微镜下手工挑选合适的磷灰石晶体(晶体最短轴直径大于75 μm的自形晶颗粒),每件样品中挑选的磷灰石颗粒大于500颗。

磷灰石颗粒的裂变径迹测试在核工业北京地质研究院分析测试研究中心完成。首先将挑选出来的磷灰石矿物颗粒用环氧树脂固定于光玻片上进行研磨和抛光处理,随后在恒温21±0.5 °C的条件下使用5.5 mol/L HNO₃溶液对其进行20 s的蚀刻来揭示自发径迹。采用外探测器法(Hurford and Gleadow, 1977)对磷灰石裂变径迹年龄进行测定,详细的测试步骤见Yuan et al. (2013)。将低铀白云母片作为外探测器盖在树脂片上,与标准铀玻璃(NIST SRM 611、613、615)、标准样品(Durango磷灰石)一起按顺序包装,在美国俄勒冈州立大学Triga反应堆进行热中子辐照。辐照后的白云母片在25°C、40%的HF中蚀刻40 min,揭示出诱发径迹;将树脂片和云母片按照镜像关系粘在玻璃片上待测量。用Carl Zeiss Axio Imager M2m显微镜在1000倍放大倍数下进行径迹观察,选择平行于C轴的颗粒测量自发径迹密度、诱发径迹密度、封闭径迹长度、D_{par}值、径迹与C轴夹角。

2.2 热史模拟方法

使用HeFTy软件(Version 1.9.3)(Ketcham, 2005)对磷灰石样品进行时间-温度(*t-T*)热史模拟。拟合曲线采用Monte Carlo逼近算法,运用多组分退火模型(Ketcham et al., 2007),并同时考虑到裂变径迹年龄、径迹长度与D_{par}值等参数。现有研究成果显示浙江东南部雁荡山地区火山机构中心侵入相岩体的锆石U-Pb年龄约为98 Ma(He et al., 2009; Yan et al., 2016)、神仙居地区火山活动时限为116~112 Ma(唐增才等, 2018),火山机构中心侵入相侵位深度约2~4 km(Yan et al., 2016; Chen et al., 2021);考虑到该时期研究区处于弧后强烈伸展区域,地温梯度为35~40 °C/km(Currie and Hyndman, 2006; Tao et al., 2019; Gan et al., 2023),而上地壳浅部(<4 km)岩浆房冷却至围岩温度的时间通常为1~4 Ma或更短(Gerdes et al., 1998; Daniels et al., 2014; 段文涛等, 2017),因此将模拟初始温度设为150±10 °C,现今地层温度设为20±3 °C。由于一个岩浆房系统通常的活动时限在3 Ma以内(Karakas et al., 2019; Klein and Le Roux, 2020),故此研究未考虑岩体结晶后深部岩浆房对其相对短暂的后续影响。基于Monte Carlo方法随机模拟了10000条热演化史路径,使用拟合优度(GOF)值衡量模拟计算的古温标值与实测

表 1 磷灰石裂变径迹分析样品采样信息表

Table 1 Elevation, location and lithology of the samples for apatite fission track analysis

样品号	取样高程	采样点位坐标		岩性
		北纬	东经	
雁荡山百岗尖地区				
BGJ-1、BGJ-2、BGJ-3		28°22'19.2"	121°03'32.0"	石英正长岩
BGJ-4、BGJ-5、BGJ-6	1072 m	28°22'20.8"	121°03'35"	石英正长岩
BGJ-7、BGJ-9	1054 m	28°22'22.0"	121°03'34.0"	石英正长岩
BGJ-10、BGJ-11	1034 m	28°22'22.9"	121°03'35.2"	石英正长岩
BGJ-13、BGJ-14、BGJ-15	1013 m	28°22'23.4"	121°03'37.5"	石英正长岩
BGJ-16、BGJ-17	993 m	28°22'23.6"	121°03'39.7"	石英正长岩
BGJ-19、BGJ-20、BGJ-21	972 m	28°22'26.3"	121°03'37.5"	石英正长岩
BGJ-22、BGJ-24	951 m	28°22'25"	121°03'39"	石英正长岩
BGJ-25、BGJ-26、BGJ-27	930 m	28°22'24.3"	121°03'43.8"	石英正长岩
BGJ-28、BGJ-29、BGJ-30	909 m	28°22'25.2"	121°03'44.0"	石英正长岩
BGJ-32、BGJ-33	888 m	28°22'26.1"	121°03'44.9"	石英正长岩
BGJ-36	867 m	28°22'18.2"	121°03'47.1"	石英正长岩
BGJ-40、BGJ-41、BGJ-42	831 m	28°22'10.6"	121°03'49.7"	石英正长岩
神仙居淡竹地区				
DZ-1、DZ-2、DZ-3	252 m	28°34'44"	120°35'16"	微细粒二长岩
DZ-4、DZ-5、DZ-6	272 m	28°34'38"	120°35'28"	细粒正长岩
DZ-7、DZ-8、DZ-9	288 m	28°34'34"	120°36'10"	细粒正长岩
DZ-10、DZ-11、DZ-12	290 m	28°34'33"	120°36'12"	微细粒二长岩
DZ-13、DZ-14、DZ-15	257 m	28°34'37"	120°35'32"	细粒正长岩
DZ-17	290 m	28°33'47"	120°35'25"	细粒正长岩
DZ-21	329 m	28°33'28"	120°35'25"	细粒正长岩
DZ-22、DZ-23、DZ-24	346 m	28°33'23"	120°35'28"	细粒正长岩
DZ-25、DZ-26、DZ-27	460 m	28°32'55"	120°35'28"	细粒正长岩
DZ-29、DZ-30	481 m	28°32'51"	120°35'28"	细粒正长岩
DZ-31	522 m	28°32'35"	120°35'27"	细粒正长岩

古温标值的拟合程度,当GOF大于50%时,认为热演化史模拟结果具有一定实际参考意义,其中拟合度最好的t-T路径最可能代表样品的热演化史。

3 磷灰石裂变径迹与热史模拟结果

3.1 磷灰石裂变径迹测试结果

对全部样品(58件)进行了磷灰石裂变径迹分析工作,具体测试结果见表2,每个样品分析的磷灰石颗粒在20至27个之间。

雁荡山百岗尖地区的32件样品的磷灰石裂变径迹年龄均通过了 χ^2 检验($P(\chi^2) \geq 0.05$),指示所有样品的磷灰石裂变径迹年龄均服从泊松分布,属于单一年龄组分(Galbraith, 1981),因此此次研究使用池年龄(Sobel et al., 2006)与中心年龄(Vermeesch, 2018)

对其进行表示。其中大多数样品(62.5%, 20件)的年龄分布于40~31 Ma,7件(21.9%)样品(BGJ-9、BGJ-10、BGJ-11、BGJ-17、BGJ-28、BGJ-30、BGJ-40)的年龄分布于50~41 Ma,仅5件(15.6%)样品(BGJ-1、BGJ-4、BGJ-5、BGJ-16、BGJ-22)的年龄分布于61~51 Ma。该地区所获磷灰石样品的平均封闭径迹长度约为11.12~14.50 μm ,平均 D_{par} 值分布于0.78~1.04 μm (表2)。

神仙居淡竹地区的26件样品的磷灰石裂变径迹年龄同样通过了 χ^2 检验($P(\chi^2) \geq 0.05$),指示其为单一组分年龄。其中61.5%的样品(16件)的年龄分布于40~31 Ma,8件(30.8%)样品(DZ-1、DZ-3、DZ-9、DZ-14、DZ-22、DZ-23、DZ-24)的年龄分布于50~41 Ma,仅2件(7.7%)样品(DZ-11、DZ-25)的年

表2 磷灰石裂变径迹测试结果表

Table 2 Results of the apatite fission track test

样品	颗粒数	$\rho_s/(\times 10^5/\text{cm}^{-2}) (N_s)$	$\rho_i/(\times 10^5/\text{cm}^{-2}) (N_i)$	$\rho_d/(\times 10^5/\text{cm}^{-2}) (N_d)$	池年龄/Ma	中心年龄/Ma	$P(\chi^2)/\%$	径迹长度/($\mu\text{m} \pm 1\text{SD}$) (N)	$D_{par}/\mu\text{m}$
DZ-1	20	0.397 (78)	0.560 (110)	50.249 (1004)	48.5 ± 8.7	48.5 ± 8.5	98	13.72 ± 0.59 (5)	1.10
DZ-2	23	0.469 (106)	1.022 (231)	50.520 (1017)	31.6 ± 4.9	31.6 ± 4.8	> 99	/	0.97
DZ-3	20	0.285 (56)	0.417 (82)	50.792 (1029)	47.2 ± 9.4	47.2 ± 9.4	> 99	12.63 ± 0.83 (3)	1.02
DZ-4	24	0.335 (79)	0.742 (175)	51.063 (1041)	31.4 ± 5.3	31.4 ± 5.2	> 99	/	1.00
DZ-5	21	0.300 (62)	0.664 (137)	51.334 (1054)	31.6 ± 5.8	31.6 ± 5.7	> 99	13.80 ± 0.61 (3)	1.03
DZ-6	21	0.528 (109)	1.226 (253)	51.605 (1066)	30.3 ± 4.6	30.3 ± 4.5	> 99	13.02 ± 0.96 (6)	1.04
DZ-7	22	0.638 (138)	1.221 (264)	51.877 (1078)	36.9 ± 5.4	36.9 ± 5.2	99	12.69 ± 0.93 (3)	0.98
DZ-8	20	0.336 (66)	0.651 (128)	52.148 (1091)	36.6 ± 6.6	36.6 ± 6.6	> 99	12.63 ± 0.95 (6)	1.06
DZ-9	20	0.290 (57)	0.509 (100)	52.419 (1103)	40.7 ± 7.9	40.7 ± 7.8	> 99	13.05 ± 0.50 (1)	1.02
DZ-10	25	0.354 (87)	0.798 (196)	52.690 (1115)	31.8 ± 5.2	31.8 ± 5.1	> 99	12.86 ± 0.72 (1)	1.00
DZ-11	24	0.343 (81)	0.407 (96)	52.962 (1128)	60.7 ± 11.0	61.0 ± 11.0	> 99	/	0.99
DZ-12	24	0.428 (101)	0.788 (186)	53.233 (1140)	39.3 ± 6.2	39.3 ± 6.1	> 99	14.44 ± 0.86 (2)	1.05
DZ-13	21	0.339 (70)	0.659 (136)	53.504 (1152)	37.5 ± 6.7	37.5 ± 6.6	> 99	13.09 ± 1.26 (4)	1.05
DZ-14	20	0.594 (53)	1.054 (94)	53.775 (1165)	41.3 ± 8.2	41.0 ± 8.1	> 99	13.00 ± 1.11 (3)	1.00
DZ-15	20	0.341 (47)	0.754 (104)	54.047 (1177)	33.3 ± 6.7	34.0 ± 7.0	> 99	/	1.00
DZ-17	20	0.674 (54)	1.423 (114)	54.589 (1202)	35.2 ± 6.8	35.2 ± 6.7	> 99	12.94 ± 0.16 (2)	0.86
DZ-21	20	0.462 (52)	0.932 (105)	55.674 (1251)	37.5 ± 7.4	37.5 ± 7.3	> 99	13.54 ± 0.18 (2)	0.90
DZ-22	21	0.750 (43)	1.204 (69)	55.945 (1263)	47.4 ± 10.3	47.0 ± 10.0	> 99	/	0.90
DZ-23	20	0.602 (43)	1.049 (75)	56.216 (1276)	43.8 ± 9.4	43.8 ± 9.4	> 99	/	1.06
DZ-24	22	0.619 (43)	1.137 (79)	56.488 (1288)	41.8 ± 8.9	41.8 ± 8.9	99	/	1.04
DZ-25	20	0.638 (42)	0.941 (62)	56.759 (1300)	52.3 ± 11.7	52.0 ± 12.0	> 99	12.11 ± 0.67 (6)	1.12
DZ-26	23	0.577 (55)	1.029 (98)	57.030 (1312)	43.5 ± 8.5	43.5 ± 8.4	> 99	/	0.99
DZ-27	20	0.447 (54)	0.820 (99)	7.085 (5668)	36.2 ± 6.7	36.2 ± 6.7	> 99	/	0.91
DZ-29	20	0.488 (53)	0.911 (99)	7.204 (5763)	36.2 ± 6.7	36.2 ± 6.7	> 99	/	1.00
DZ-30	21	0.710 (40)	1.243 (70)	7.264 (5811)	38.9 ± 8.3	38.9 ± 8.2	> 99	12.77 ± 0.88 (4)	0.96
DZ-31	20	0.654 (46)	1.236 (87)	7.324 (5859)	36.3 ± 7.2	36.3 ± 7.1	> 99	/	1.02
BGJ-1	27	1.316 (127)	1.533 (148)	7.503 (6003)	60.2 ± 8.6	61.0 ± 9.0	41	13.23 ± 0.62 (2)	0.98
BGJ-2	20	1.078 (123)	2.007 (229)	7.563 (6050)	38.1 ± 5.1	38.1 ± 5.1	> 99	13.23 ± 1.96 (3)	1.04
BGJ-3	20	1.123 (122)	2.016 (219)	7.623 (6098)	39.8 ± 5.4	39.8 ± 5.4	> 99	12.66 ± 0.95 (1)	1.04
BGJ-4	21	0.784 (45)	1.115 (64)	7.682 (6145)	50.6 ± 10.6	51.0 ± 11.0	97	/	0.93
BGJ-5	20	0.901 (63)	1.087 (76)	7.742 (6193)	60.0 ± 11.2	60.0 ± 11.0	> 99	12.63 ± 1.62 (6)	0.98
BGJ-6	20	0.908 (55)	1.850 (112)	7.802 (6242)	35.9 ± 6.5	35.9 ± 6.5	> 99	12.36 ± 0.45 (3)	0.92
BGJ-7	21	0.649 (53)	1.347 (110)	7.862 (6289)	35.5 ± 6.5	35.5 ± 6.5	> 99	12.26 ± 0.01 (2)	0.97
BGJ-9	20	0.538 (43)	0.938 (75)	7.981 (6385)	42.9 ± 8.8	42.9 ± 8.8	> 99	12.50 ± 0.30 (3)	0.92
BGJ-10	21	0.671 (40)	1.192 (71)	8.041 (6433)	42.4 ± 9.0	42.1 ± 9.1	> 99	/	0.98
BGJ-11	20	0.675 (43)	1.130 (72)	8.101 (6481)	45.3 ± 9.4	45.3 ± 9.4	> 99	/	1.00
BGJ-13	22	0.656 (58)	1.358 (120)	8.220 (6576)	37.2 ± 6.6	37.2 ± 6.6	> 99	/	1.00
BGJ-14	25	0.760 (83)	1.850 (202)	8.280 (6624)	31.9 ± 4.8	31.9 ± 4.8	89	14.09 ± 1.08 (4)	1.03
BGJ-15	20	0.674 (54)	1.435 (115)	8.340 (6672)	36.7 ± 6.7	36.7 ± 6.6	> 99	/	0.94

续表 2

样品	颗粒数	$\rho_s/(\times 10^5/\text{cm}^{-2}) (N_s)$	$\rho_i/(\times 10^5/\text{cm}^{-2}) (N_i)$	$\rho_d/(\times 10^5/\text{cm}^{-2}) (N_d)$	池年龄/Ma	中心年龄/Ma	$P(\chi^2)/\%$	径迹长度/($\mu\text{m} \pm 1\text{SD}$) (N)	$D_{\text{par}}/\mu\text{m}$
BGJ-16	20	0.963 (41)	1.410 (60)	8.399 (6720)	53.7 ± 11.6	54.0 ± 12.0	> 99	/	0.88
BGJ-17	23	0.586 (60)	1.075 (110)	8.459 (6767)	43.2 ± 7.7	43.2 ± 7.6	> 99	/	0.92
BGJ-19	21	0.961 (90)	1.569 (147)	0.159 (794)	39.3 ± 6.5	39.4 ± 6.4	93	12.75 ± 0.43 (1)	0.90
BGJ-20	22	0.710 (63)	1.183 (105)	0.159 (797)	38.7 ± 7.2	39.0 ± 7.0	> 99	/	0.91
BGJ-21	21	0.748 (52)	1.439 (100)	0.160 (801)	33.7 ± 6.6	33.7 ± 6.5	> 99	13.10 ± 0.05 (1)	0.90
BGJ-22	20	0.804 (43)	0.935 (50)	0.161 (804)	55.8 ± 12.8	56.0 ± 13.0	> 99	14.50 ± 0.53 (2)	0.78
BGJ-24	24	0.715 (77)	1.374 (148)	0.162 (810)	34.1 ± 5.8	34.1 ± 5.7	99	11.12 ± 0.24 (3)	0.96
BGJ-25	20	0.807 (61)	1.720 (130)	0.163 (814)	30.9 ± 5.6	30.9 ± 5.5	99	/	0.92
BGJ-26	20	0.705 (50)	1.467 (104)	0.163 (817)	31.8 ± 6.3	31.7 ± 6.1	> 99	/	0.96
BGJ-27	20	0.666 (68)	1.264 (129)	0.164 (820)	35.0 ± 6.2	35.0 ± 6.1	> 99	13.14 ± 1.05 (1)	0.90
BGJ-28	20	0.778 (38)	1.269 (62)	0.165 (823)	40.8 ± 9.3	40.9 ± 9.2	> 99	/	0.86
BGJ-29	24	0.717 (86)	1.425 (171)	0.165 (826)	33.6 ± 5.5	33.6 ± 5.3	> 99	12.39 ± 0.36 (2)	0.80
BGJ-30	21	0.652 (53)	1.021 (83)	0.166 (830)	42.8 ± 8.6	42.9 ± 8.4	> 99	13.05 ± 0.31 (4)	0.82
BGJ-32	21	0.716 (43)	1.215 (73)	0.167 (836)	39.8 ± 8.5	39.8 ± 8.4	> 99	12.43 ± 0.52 (1)	0.95
BGJ-33	20	0.710 (47)	1.330 (88)	0.168 (839)	36.2 ± 7.4	36.3 ± 7.3	> 99	11.99 ± 0.88 (1)	0.93
BGJ-36	22	0.581 (54)	1.087 (101)	0.170 (849)	36.7 ± 7.1	37.0 ± 7.0	99	12.50 ± 1.12 (4)	0.92
BGJ-40	20	0.992 (43)	1.661 (72)	0.172 (862)	41.6 ± 8.9	41.5 ± 8.8	> 99	/	0.90
BGJ-41	22	0.765 (86)	1.744 (196)	0.173 (865)	30.7 ± 4.9	30.7 ± 4.8	> 99	14.04 ± 0.45 (1)	0.84
BGJ-42	22	0.564 (74)	1.189 (156)	0.174 (868)	33.3 ± 5.7	33.3 ± 5.6	> 99	/	0.90

注: 表中 N_s 为自发径迹数, N_i 为诱发径迹数, N_d 为标准玻璃的外探测器白云母记录的径迹数; ρ_s 、 ρ_i 、 ρ_d 分别表示与 N_s 、 N_i 、 N_d 相对应的径迹密度; $P(\chi^2)$ 为 χ^2 检验值; N 表示径迹条数; 池年龄与中心年龄误差范围均以1个标准误差值(1SD)表示

龄分布于51~61 Ma。该地区所获磷灰石样品的平均封闭径迹长度约为12.11~14.44 μm , 平均 D_{par} 值分布于0.86~1.12 μm (表2)。

2个地区所有磷灰石裂变径迹单颗粒年龄(除去极少部分裂变径迹年龄大于成岩年龄的不合理单颗粒磷灰石数据)进的频谱成图与统计显示,二者具有几乎完全一致的年龄分布规律,均呈典型的单峰式分布样式,峰值均位于约33 Ma处;此外,在约70 Ma附近二者均有一个略高于平均值的较低峰存在(图4)。

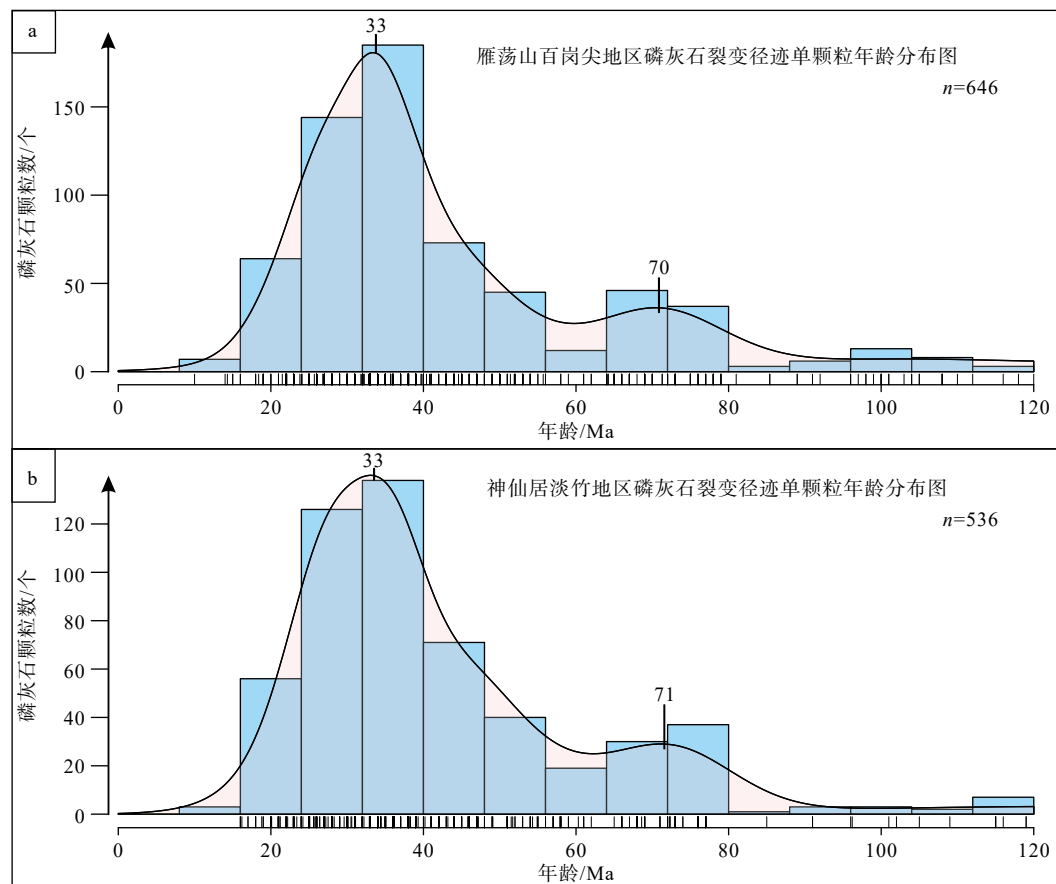
3.2 磷灰石裂变径迹热史模拟结果

磷灰石裂变径迹表观年龄仅代表了样品通过其部分退火带(60~120 °C)的时间(Reiners and Brandon, 2006; Lisker et al., 2009),而其裂变径迹数据包含的热历史信息往往需要通过热史模拟来进一步挖掘(Ketcham et al., 2007; Gallagher, 2012)。此次研究的样品由于自发径迹密度较低,单件样品难以获取足够的封闭径迹长度数据。但鉴于2个地区样品采样距离近、相对高程差较小、岩性一致且来

自同一火山机构、采样区域内无深大断裂且各样品中心年龄在误差范围内均一致,故对雁荡山百岗尖地区BGJ-1至BGJ-30号样品(高程1000±100 m)和神仙居淡竹地区DZ-1至DZ-24号样品(高程300±50 m)的径迹长度数据分别进行合并,再分别对这些样品进行HeFTy热史模拟,最后将每件样品模拟所获得的最佳拟合曲线(GOF值最大)汇总成图(图5)。

雁荡山百岗尖地区样品(BGJ-1至BGJ-30)的裂变径迹长度呈典型单峰式分布,平均长度为12.8±1.1 μm (图5)。热史模拟结果显示,该地区的石英正长岩样品在侵位后首先经历了一个缓慢冷却至磷灰石裂变径迹部分退火带之下或完全退火临界值温度附近(T_A , ~120 °C; Reiners and Brandon, 2006)的过程,该阶段样品的冷却速率较为缓慢(约0.4~0.8 °C/Ma);始新世早期—渐新世最早期(约48 Ma~33 Ma),样品经历了一个快速抬升冷却至磷灰石裂变径迹部分退火带温度之上的过程,冷却速率为8~20 °C/Ma。

对于神仙居淡竹地区的样品(DZ-1至DZ-24),



a—雁荡山地区单颗粒磷灰石裂变径迹年龄分布直方-频谱图; b—神仙居地区单颗粒磷灰石裂变径迹年龄分布直方-频谱图(n 为统计的磷灰石颗粒数)

图4 浙东南部火山岩分布区单颗粒磷灰石裂变径迹年龄分布直方-频谱图

Fig. 4 Histograms and probability density curves of single grain apatite fission track ages from the volcanic areas in southeastern Zhejiang (n is the number of analyzed apatite grains)

(a) Histogram and probability density curve of single-grain apatite fission track ages from the Yandang Mountain area; (b) Histogram and probability density curve of single-grain apatite fission track ages from the Shenxianju area

其径迹分布同样为典型单峰式分布, 平均径迹长为 $12.9 \pm 1.3 \mu\text{m}$ (图5)。热史模拟结果显示, 该地区的样品在侵位后首先经历了缓慢抬升冷却至完全退火临界值温度之下 (T_A , $\sim 120^\circ\text{C}$) 的过程或长期保持稳定在磷灰石部分退火带的底部温度附近 ($100 \sim 120^\circ\text{C}$); 始新世早期—渐新世最早期 (约 52 Ma \sim 32 Ma), 样品被快速抬升至磷灰石裂变径迹部分退火带温度之上, 冷却速率为 $5 \sim 16^\circ\text{C}/\text{Ma}$ 。

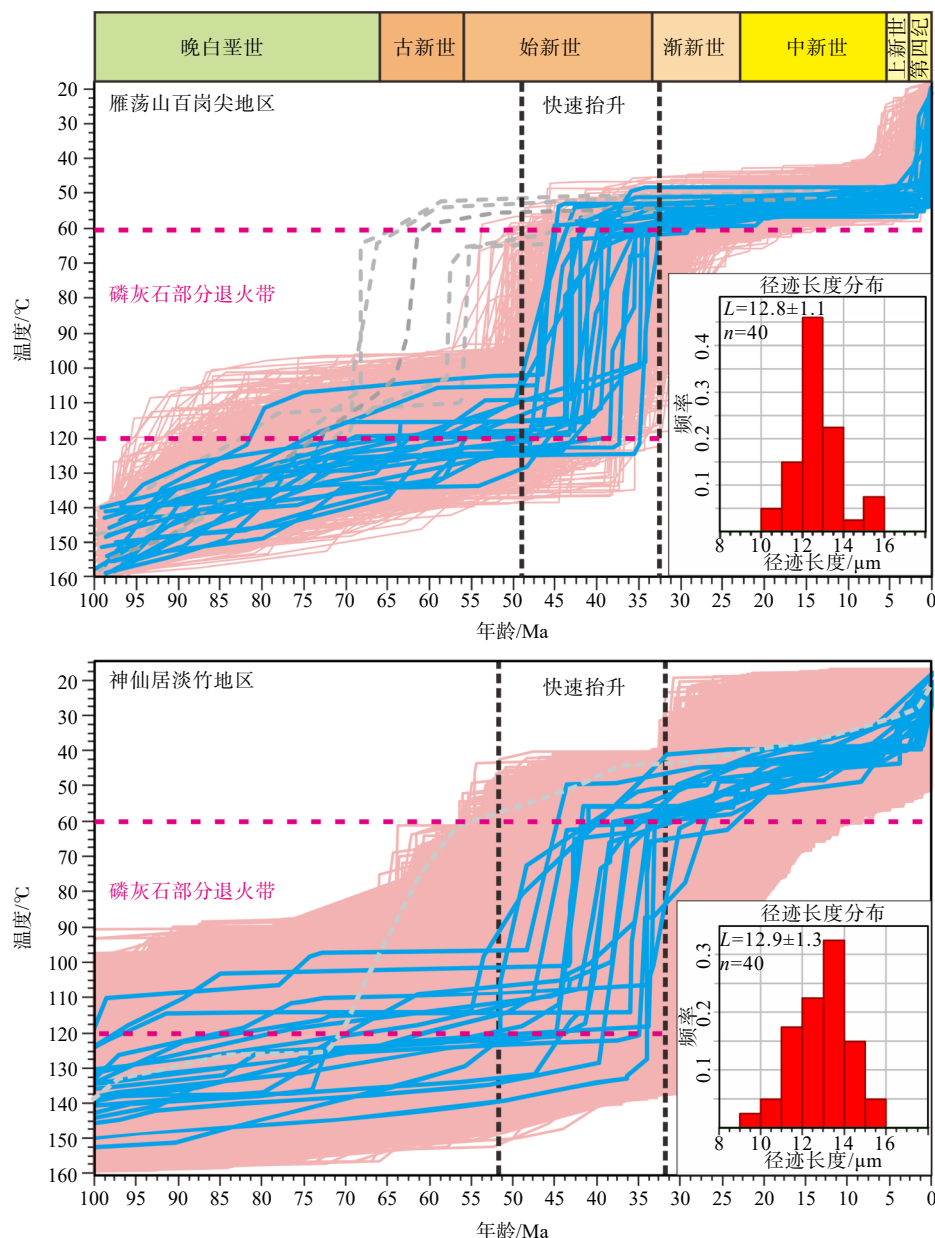
4 讨论

4.1 数据解释与区域抬升历史

上地壳浅部 ($< 4 \text{ km}$) 侵入岩与围岩达到热平衡所需时间通常为 $1 \sim 4 \text{ Ma}$ 或更短 (Gerdes et al., 1998; Daniels et al., 2014), 2个地区样品的磷灰石裂

变径迹年龄均显著年轻于其侵位年龄 (雁荡山百岗尖石英正长岩为 $96 \sim 100 \text{ Ma}$; 淡竹神仙居正长岩—二长岩为 $112 \sim 116 \text{ Ma}$), 指示其代表了后期的抬升冷却事件, 而非侵位后岩浆快速冷却过程。

热年代学数据显示, 2个地区的磷灰石裂变径迹年龄具有高度一致的分布规律, 其中心年龄与合并年龄多集中于 $40 \sim 31 \text{ Ma}$ (雁荡山百岗尖地区为 62.5%、神仙居淡竹地区为 64%), 部分分布于 $50 \sim 41 \text{ Ma}$ (雁荡山百岗尖地区为 21.9%、神仙居淡竹地区为 30.8%), 少量分布于 $61 \sim 50 \text{ Ma}$ (雁荡山百岗尖地区为 15.6%、神仙居淡竹地区为 7.7%); 二者的单颗粒磷灰石裂变径迹年龄频谱图均表现为单峰式分布, 峰值均位于 33 Ma 附近 (图4); 从 HeFTy 热史模拟结果上来看, 二者均在始新世早期—渐新世最早期经历了 1 期快速的冷却事件, 均具有较快



图中蓝色曲线为各次模拟的最佳曲线;粉色曲线代表 GOF 值大于 0.5 的模拟曲线;灰色虚线为个别与多数最佳模拟曲线偏离较大的结果;径迹长度分布图中 L 代表径迹加权平均长度, n 代表统计的径迹条数

图 5 雁荡山与神仙居地区样品磷灰石裂变径迹 HeFTy 热史模拟最佳拟合曲线汇总图

Fig. 5 Best-fit thermal history curves for samples from Yandang Mountain and Shenxianju area generated in HeFTy (Ketcham et al., 2007) based on apatite fission track data

Solid blue lines represent the best-fit models of each specimen; solid pink lines show the "good" thermal history paths ($GOF > 0.5$); grey dash-lines represent minor best-fit models deviate from the major group; L is the weighted mean length of the apatite fission tracks, n is the number of analyzed apatite fission tracks.

的冷却速率($8 \sim 20^{\circ}\text{C/Ma}$ 和 $5 \sim 16^{\circ}\text{C/Ma}$)。根据以上结果,认为雁荡山百岗尖地区与神仙居淡竹地区具有相似的抬升冷却历史,自始新世早期(约 52 ~ 48 Ma)起经历了 1 期快速抬升冷却事件,由磷灰石部分退火带的高温临界值($\sim 120^{\circ}\text{C}$)开始抬升,至始新世末期—渐新世最早期(34 ~ 32 Ma)抬升至磷

灰石部分退火带的上限温度附近(约 60°C)。

4.2 区域构造意义

中国东南沿海地区是西太平洋洋陆过渡带的重要组成部分(Li et al., 2019; Suo et al., 2019),自中生代以来经历了多期复杂的构造演化过程(Ren et al., 2002; Suo et al., 2019, 2020),其抬升冷却历史具

有重要地质意义。学者们针对东南沿海及其邻近的内陆地区已开展了大量的低温热年代学研究(Li et al., 2005, 2016; Yi et al., 2009; Tang et al., 2014; Li and Zou, 2017; Su et al., 2017; Tao et al., 2017; Ding et al., 2019; Wang et al., 2020, 2022), 总体来看, 该地区在早白垩世末期—晚白垩世早期(110~85 Ma), 晚白垩世末期—始新世早期(70~50 Ma)和始新世晚期—渐新世(40~25 Ma)存在3期区域性抬升冷却事件。但研究数据多集中于广东、福建、海南和江西等地区, 而对浙江地区低温热年代学数据报道较少。Wang et al. (2015)对江绍断裂带陈蔡地区开展了锆石-磷灰石裂变径迹研究, 获得其锆石裂变径迹年龄为144~103 Ma, 而磷灰石裂变径迹年龄为66~41 Ma, 其HeFTy热历史模拟结果显示陈蔡地区的基底岩石在约50~35 Ma期间经历了1期较为快速的抬升。王新毓等(2020)在浙江省金华金东区至台州天台县一带进行了系统的磷灰石裂变径迹年代学研究, 其样品主要的磷灰石裂变径迹年龄集中于39~31 Ma, 少量靠近丽水-余姚断裂带的样品记录了27~25 Ma及~19 Ma的磷灰石裂变径迹年龄, HeFTy热历史模拟结果显示该研究区在38~29 Ma、27~12 Ma和~5 Ma至今经历了3期快速抬升。而此次雁荡山、神仙居地区获得的大量磷灰石裂变径迹年龄多数集中于50~31 Ma, 峰值约为33 Ma, 热历史模拟结果显示该地区快速抬升时限在约50~32 Ma。综合以上数据, 认为浙江省在始新世早期—渐新世早期(50~31 Ma)期间普遍经历了1次区域抬升作用。

始新世早期—渐新世早期(50~31 Ma), 华南地块的东部和西部边界均经历了重大的构造格局变动。东部构造域, 伊泽那崎-古太平洋板块洋脊在53~47 Ma发生了平行于海沟的俯冲(Seton et al., 2015; Müller et al., 2016), 引发了东亚大陆边缘短暂的区域挤压变形、弧岩浆活动的间断及区域地温梯度扰动等一系列地质事件(Seton et al., 2015; Zhu et al., 2019); 随后(约46~35 Ma), 洋脊俯冲至软流圈形成板片窗, 导致强烈的弧后地幔上涌、弧后区域伸展事件(李三忠等, 2019; Wang et al., 2022; Tian et al., 2025)。而在西部构造域, 印度与欧亚板块于61~59 Ma发生陆-陆碰撞(Hu et al., 2015; An et al., 2021), 两大板块的持续汇聚导致欧亚大陆(包括华南地块)在始新世晚期—渐新世早期(约34~29 Ma)开始形成向东逃逸-挤出构造, 并伴随东向地幔

流(Tapponnier et al., 1982; Leloup et al., 2001; Akciz et al., 2008; Cao et al., 2011; Schellart et al., 2019)。以上动力学过程引发了华南板块向东移动, 并导致东部陆缘发生1期短暂的挤压-反转构造事件(王新毓等, 2020; Zhang et al., 2021)。与此同时, 太平洋板块俯冲后撤在弧后地区诱发大规模地幔上涌, 并形成拉分盆地构造(Fournier et al., 2004; Schellart et al., 2019; Zhang et al., 2019)。因此研究认为, 浙江地区在始新世中期—渐新世早期的区域性持续抬升过程具有明显的阶段性特征: 早期主要受控于华南地块东部伊泽那崎-太平洋板块洋脊的俯冲作用, 而晚期则主要受到西部印度-欧亚大陆的持续汇聚导致的远程效应与太平洋板块俯冲后撤的共同作用(图6)。值得注意的是, 尽管起始于始新世中期(约40 Ma)的东亚季风可加快其影响区域的岩石剥蚀速率而加速岩石的冷却(Licht et al., 2014; Wang et al., 2022), 但考虑到始新世期间东亚季风的影响范围主要局限于华南板块南缘的低纬度地区(Guo et al., 2008; Xie et al., 2019; 林旭等, 2024), 且此次研究得到的岩石快速剥露起始时间早于东亚季风的起始时限(Guo et al., 2008; Licht et al., 2014; Xie et al., 2019), 因此认为东亚季风并非研究区在始新世早期—渐新世早期(50~31 Ma)快速隆升-剥露的主要因素。

5 结论

研究报道了浙东南地区白垩纪火山机构中心相侵入体的磷灰石裂变径迹年龄, 为该区新生代构造与地貌演化过程提供了重要约束, 形成了以下主要认识。

(1) 雁荡山与神仙居破火山构造中心相侵入岩的磷灰石裂变径迹年龄分布于61~31 Ma之间, 其中多数集中在40~31 Ma, 其次为50~41 Ma, 仅少量分布于61~51 Ma;

(2) 雁荡山地区与神仙居地区在始新世早期(约52~48 Ma)至渐新世最早期(34~32 Ma)经历了1期快速抬升冷却事件, 该抬升事件早期的动力学来源认为主要是伊泽那崎-太平洋板块洋脊的俯冲作用, 晚期则是受印度-欧亚大陆碰撞汇聚的远程效应与太平洋板块俯冲后撤的共同影响, 导致发生了该期快速抬升冷却。

由于目前研究仅局限于浙东南雁荡山和神仙

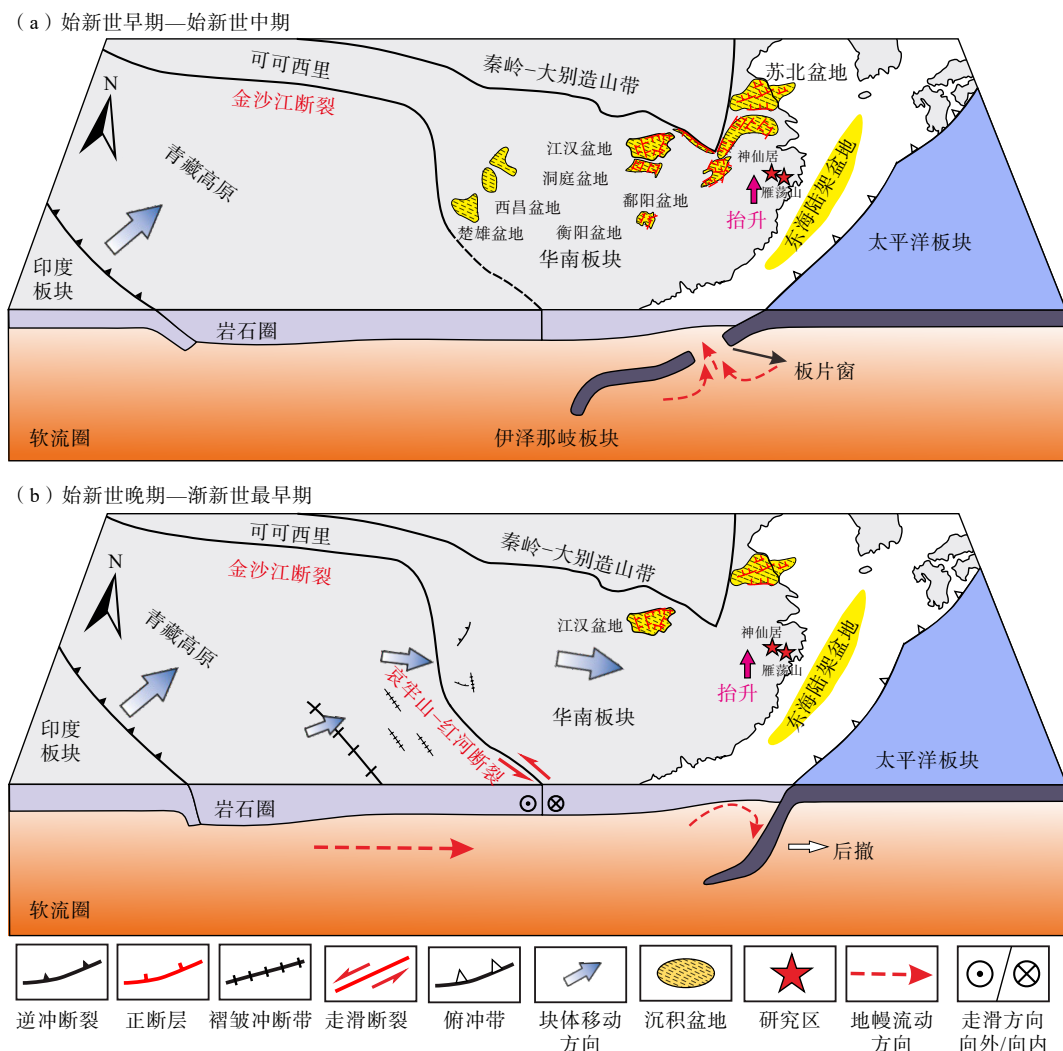


图 6 始新世早期—渐新世最早期东南沿海及其周边地区大地构造模式简图 (据 Tian et al., 2025 修改)

Fig. 6 Schematic block diagram showing the tectonic model of the southeastern coastal region of China and adjacent areas during the Early Eocene–Earliest Oligocene (modified after Tian et al., 2025)

(a) Early Eocene – Middle Eocene; (b) Late Eocene – Earliest Oligocene

居地区,且方法较为单一,后续研究团队将在更大区域范围上开展更为全面的低温热年代学与构造地貌研究工作,从而进一步完善研究成果。

致谢:浙江省水文地质工程地质大队(浙江省宁波地质院)唐小明教授级高工对前期研究工作进行了指导,浙江省地矿科技有限公司游省易高级工程师、张君工程师参与了前期野外调查和样品采集工作,山东大学郑文浩博士参与了前期测试数据整理分析工作,审稿人对本文撰写提出了宝贵修改意见,在此一并致谢。

References

- AKCIZ S, BURCHFIELD B C, CROWLEY J L, et al., 2008. Geometry, kinematics, and regional significance of the Chong Shan shear zone, eastern Himalayan Syntaxis, Yunnan, China[J]. *Geosphere*, 4(1): 292-314.
 AN W, HU X M, GARZANTI E, et al., 2021. New precise dating of the India-Asia collision in the Tibetan Himalaya at 61 Ma[J]. *Geophysical Research Letters*, 48(3): e2020GL090641.
 CAO S Y, LIU J L, LEI S B, et al., 2011. Oligo-Miocene shearing along the Ailao Shan-Red River shear zone: constraints from structural analysis and zircon U/Pb geochronology of magmatic rocks in the Diancang Shan massif, SE Tibet, China[J]. *Gondwana Research*, 19(4): 975-993.
 CHEN J Y, YANG J H, ZHANG J H, et al., 2021. Construction of a highly silicic upper crust in southeastern China: insights from the cretaceous intermediate-to-felsic rocks in eastern Zhejiang[J]. *Lithos*, 402-403: 106012.
 CURRIE, C. A., & HYNDMAN, R. D., 2006. The thermal structure of subduction zone back arcs. *Journal of Geophysical Research: Solid Earth*, 111(B8).
 DANIELS K A, BASTOW I D, KEIR D, et al., 2014. Thermal models of dyke intrusion during development of continent-ocean transition[J]. *Earth*

- and Planetary Science Letters, 385: 145-153.
- DING R X, MIN K, ZOU H P, 2019. Inversion of topographic evolution using low-T thermal history: a case study from coastal mountain system in southeastern China[J]. *Gondwana Research*, 67: 21-32.
- DONG S W, LI J H, GAO R, et al., 2023. Intralate lithospheric extension revealed by seismic reflection profiling of South China[J]. *Earth and Planetary Science Letters*, 609: 118100.
- DUAN W T, HUANG S P, TANG X Y, et al., 2017. Numerical simulation of the thermal diffusion of volcanic magmatism with ANSYS WORKBENCH[J]. *Acta Petrologica Sinica*, 33(1): 267-278. (in Chinese with English abstract)
- DUAN Z, ZHAO X L, XING G F, et al., 2015. Comparison study of petrogeneses and crust-mantle interactions between cretaceous lower and upper volcanic series in the adjacent area of Zhejiang-Fujian provinces[J]. *Acta Geologica Sinica*, 89(2): 319-338. (in Chinese with English abstract)
- FANG Y, ZOU H, BAGAS L, et al., 2020. Fluorite deposits in the Zhejiang Province, Southeast China: the possible role of extension during the late stages in the subduction of the Paleo-Pacific oceanic plate, as indicated by the Gudongkeng fluorite deposit[J]. *Ore Geology Reviews*, 117: 103276.
- FOURNIER M, JOLIVET L, DAVY P, et al., 2004. Backarc extension and collision: an experimental approach to the tectonics of Asia[J]. *Geophysical Journal International*, 157(2): 871-889.
- GALBRAITH R F, 1981. On statistical models for fission track counts[J]. *Journal of the International Association for Mathematical Geology*, 13(6): 471-478.
- GALLAGHER K, 2012. Transdimensional inverse thermal history modeling for quantitative thermochronology[J]. *Journal of Geophysical Research: Solid Earth*, 117(B2): B02408.
- GAN H N, WANG X, WANG B, et al., 2023. Cenozoic thermal rheological evolution of the coastal cathaysia block of East Asia: geodynamic implications[J]. *International Geology Review*, 65(16): 2580-2593.
- GERDES M L, BAUMGARTNER L P, PERSON M, 1998. Convective fluid flow through heterogeneous country rocks during contact metamorphism[J]. *Journal of Geophysical Research: Solid Earth*, 103(B10): 23983-24003.
- GUO Z T, SUN B, ZHANG Z S, et al., 2008. A major reorganization of Asian climate by the early Miocene[J]. *Climate of the Past*, 4(3): 153-174.
- HE Z Y, XU X S, YU Y, et al., 2009. Origin of the Late Cretaceous syenite from Yandangshan, SE China, constrained by zircon U-Pb and Hf isotopes and geochemical data[J]. *International Geology Review*, 51(6): 556-582.
- HU X M, GARZANTI E, MOORE T, et al., 2015. Direct stratigraphic dating of India-Asia collision onset at the Selendian (middle Paleocene, 59±1 Ma)[J]. *Geology*, 43(10): 859-862.
- HURFORD A J, GLEADOW A J W, 1977. Calibration of fission track dating parameters[J]. *Nuclear Track Detection*, 1(1): 41-48.
- KARAKAS O, WOTZLAW J F, GUILLONG M, et al., 2019. The pace of crustal-scale magma accretion and differentiation beneath silicic caldera volcanoes[J]. *Geology*, 47(8): 719-723.
- KETCHAM R A, 2005. Forward and inverse modeling of low-temperature thermochronometry data[J]. *Reviews in mineralogy and geochemistry*, 58(1): 275-314.
- KETCHAM R A, CARTER A, DONELICK R A, et al., 2007. Improved modeling of fission-track annealing in apatite[J]. *American Mineralogist*, 92(5-6): 799-810.
- KLEIN F, LE ROUX V, 2020. Quantifying the volume increase and chemical exchange during serpentinization[J]. *Geology*, 48(6): 552-556.
- LAPIERRE H, JAHN B M, CHARVET J, et al., 1997. Mesozoic felsic arc magmatism and continental olivine tholeiites in Zhejiang Province and their relationship with the tectonic activity in southeastern China[J]. *Tectonophysics*, 274(4): 321-338.
- LAPIERRE H, JAHN B M, CHARVET J, et al., 1997. Mesozoic felsic arc magmatism and continental olivine tholeiites in Zhejiang province and their relationship with the tectonic activity in southeastern China[J]. *Tectonophysics*, 274(4): 321-338.
- LELOUP P H, ARNAUD N, LACASSIN R, et al., 2001. New constraints on the structure, thermochronology, and timing of the Ailao Shan-Red River shear zone, SE Asia[J]. *Journal of Geophysical Research: Solid Earth*, 106(B4): 6683-6732.
- LI J H, ZHANG Y Q, DONG S W, et al., 2014. Cretaceous tectonic evolution of South China: a preliminary synthesis[J]. *Earth-Science Reviews*, 134: 98-136.
- LI J H, SHI W, ZHANG Y Q, et al., 2016. Thermal evolution of the Hengshan extensional dome in central South China and its tectonic implications: new insights into low-angle detachment formation[J]. *Gondwana Research*, 35: 425-441.
- LI J H, DONG S W, GAO R, et al., 2022a. The thinnest crust in South China associated with the Cretaceous lithospheric extension: evidence from SINOPROBE seismic reflection profiling[J]. *Tectonics*, 41(8): e2022TC007240.
- LI S Z, SUO Y H, LIU B, 2018. Submarine tectonic system (volume one)[M]. Beijing: Science Press. (in Chinese)
- LI S Z, CAO X Z, WANG G Z, et al., 2019. Meso-Cenozoic tectonic evolution and plate reconstruction of the Pacific Plate[J]. *Journal of Geomechanics*, 25(5): 642-677. (in Chinese with English abstract)
- LI S Z, SUO Y H, LI X Y, et al., 2019. Mesozoic tectono-magmatic response in the East Asian ocean-continent connection zone to subduction of the paleo-pacific plate[J]. *Earth-Science Reviews*, 192: 91-137.
- LI X M, WANG Y J, TAN K X, et al., 2005. Meso-Cenozoic uplifting and exhumation on Yunkaidashan: evidence from fission track thermochronology[J]. *Chinese Science Bulletin*, 50(9): 903-909.
- LI X M, ZOU H P, 2017. Late Cretaceous-Cenozoic exhumation of the southeastern margin of Coastal Mountains, SE China, revealed by fission-track thermochronology: implications for the topographic evolution[J]. *Solid Earth Sciences*, 2(3): 79-88.
- LI X Y, LI S Z, SUO Y H, et al., 2022b. High-silica rhyolites in the terminal stage of massive Cretaceous volcanism, SE China: modified crustal sources and low-pressure magma chamber[J]. *Gondwana Research*, 102: 133-150.
- LI Z X, Li X H, 2007. Formation of the 1300-km-wide intracontinental orogen and postorogenic magmatic province in Mesozoic South China: a flat-slab subduction model[J]. *Geology*, 35(2): 179-182.
- LICHT A, VAN CAPPELLE M, ABELS H A, et al., 2014. Asian monsoons in a late Eocene greenhouse world[J]. *Nature*, 513(7519): 501-506.

- LIN X, WU Z H, DONG Y Y, et al., 2024. The evolutionary process of Cenozoic Asian monsoon[J]. *Journal of Geomechanics*, 30(4): 673-690. (in Chinese with English abstract)
- LISKER F, VENTURA B, GLASMACHER U A, 2009. Apatite thermochronology in modern geology[M]//LISKER F, VENTURA B, GLASMACHER U A. *Thermochronological methods: from palaeotemperature constraints to landscape evolution models*. London: Geological Society, London, Special Publications, 324(1): 1-23.
- LIU L, XU X S, XIA Y, 2014. Cretaceous pacific plate movement beneath SE China: evidence from episodic volcanism and related intrusions[J]. *Tectonophysics*, 614: 170-184.
- MÜLLER R D, SETON M, ZAHIROVIC S, et al., 2016. Ocean basin evolution and global-scale plate reorganization events since Pangea breakup[J]. *Annual Review of Earth and Planetary Sciences*, 44: 107-138.
- REINERS P W, BRANDON M T, 2006. Using thermochronology to understand orogenic erosion[J]. *Annual Review of Earth and Planetary Sciences*, 34: 419-466.
- REN J Y, TAMAKI K, LI S T, et al., 2002. Late Mesozoic and Cenozoic rift-ing and its dynamic setting in eastern China and adjacent areas[J]. *Tectonophysics*, 344(3-4): 175-205.
- RUAN H H, TAO K Y, XU Z L, 1988. Volcanic structure in Kuocangshan district of Zhejiang[J]. *Bull. Nanjing Inst. Geol. M. R.*, Chinese Acad. Geol. Sci., 9(2): 81-94. (in Chinese with English abstract)
- RUAN H H, XIE J Y, TAO K Y, 1993. Circular mega Volcanic structure in Kuocangshan & it's geological significance[J]. *Volcanology & Mineral Resources*, 14(4): 1-11. (in Chinese with English abstract)
- SCHELLART W P, CHEN Z, STRAK V, et al., 2019. Pacific subduction control on Asian continental deformation including Tibetan extension and eastward extrusion tectonics[J]. *Nature Communications*, 10(1): 4480.
- SETON M, FLAMENT N, WHITTAKER J, et al., 2015. Ridge subduction sparked reorganization of the Pacific plate-mantle system 60-50 million years ago[J]. *Geophysical Research Letters*, 42(6): 1732-1740.
- SHUI T, XU B T, LIANG R H, et al., 1986. Shaoxing-Jiangshan paleocontinent junction zone[J]. *Chinese Science Bulletin*, 31(6): 444-448. (in Chinese)
- SHUI T, 1988. Tectonic framework of the continental basement of Southeast China[J]. *Science China (Series B)*, 31(7): 885-896.
- SOBEL E R, OSKIN M, BURBANK D, et al., 2006. Exhumation of basement-cored uplifts: example of the Kyrgyz Range quantified with apatite fission track thermochronology[J]. *Tectonics*, 25(2): TC2008.
- SU J B, DONG S W, ZHANG Y Q, et al., 2017. Apatite fission track geochronology of the southern Hunan province across the Shi-Hang Belt: insights into the Cenozoic dynamic topography of South China[J]. *International Geology Review*, 59(8): 981-995.
- SUO Y H, LI S Z, JIN C, et al., 2019. Eastward tectonic migration and transition of the Jurassic-Cretaceous Andean-type continental margin along Southeast China[J]. *Earth-Science Reviews*, 196: 102884.
- SUO Y H, LI S Z, CAO X Z, et al., 2020. Mesozoic-Cenozoic basin inversion and geodynamics in East China: a review[J]. *Earth-Science Reviews*, 210: 103357.
- TANG D L K, SEWARD D, WILSON C J N, et al., 2014. Thermotectonic history of SE China since the Late Mesozoic: insights from detailed thermochronological studies of Hong Kong[J]. *Journal of the Geological Society*, 171(4): 591-604.
- TANG Z C, DONG X F, MENG X S, et al., 2018. Geochronology and geochemistry of Cretaceous rhyolites in the Shenxianju area, Zhejiang province[J]. *Journal of Stratigraphy*, 42(2): 167-178. (in Chinese with English abstract)
- TAO K Y, YU M G, XING G F, et al., 2004. The value and global comparison of the Cretaceous Mt. Yandangshan caldera geologic heritage[J]. *Resources Survey & Environment*, 25(4): 297-303. (in Chinese with English abstract)
- TAO N, LI Z X, DANIŠÍK M, et al., 2017. Thermochronological record of Middle-Late Jurassic magmatic reheating to Eocene rift-related rapid cooling in the SE South China Block[J]. *Gondwana Research*, 46: 191-203.
- TAO N, LI Z X, DANIŠÍK M, et al., 2019. Post-250 Ma thermal evolution of the central Cathaysia Block (SE China) in response to flat-slab subduction at the proto-western Pacific margin[J]. *Gondwana Research*, 75: 1-15.
- TAPPONNIER P, PELTZER G, LE DAIN A Y, et al., 1982. Propagating extrusion tectonics in Asia: new insights from simple experiments with plas-ticine[J]. *Geology*, 10(12): 611-616.
- TIAN Z H, SUO Y H, DING X S, et al., 2025. Cenozoic surface Earth system evolution and dynamic palaeogeomorphic reconstruction from the Tibet Plateau to the western Pacific linked by the Yangtze River[J]. *Journal of the Geological Society*, 183(2): jgs2023-183.
- VERMEESCH P, 2018. IsoplotR: a free and open toolbox for geochronology[J]. *Geoscience Frontiers*, 9(5): 1479-1493.
- WANG F, CHEN H L, BATT G E, et al., 2015. Tectonothermal history of the NE Jiangshan-Shaoxing suture zone: evidence from $^{40}\text{Ar}/^{39}\text{Ar}$ and fission-track thermochronology in the Chencai region[J]. *Precambrian Research*, 264: 192-203.
- WANG X Y, SUO Y H, LI S Z, et al., 2020. Cenozoic uplift history and its dynamic mechanism along the eastern continental margin of South China[J]. *Acta Petrologica Sinica*, 36(6): 1803-1820. (in Chinese with English abstract)
- WANG X Y, XU X S, ZHAO K., 2023. Petrogenesis of episodic Cretaceous volcanic-intrusive rocks in the Kuocangshan-Yandangshan Calderas in the eastern Zhejiang[J]. *Bulletin of Mineralogy, Petrology and Geochemistry*, 42(5): 1062-1077. (in Chinese with English abstract)
- WANG Y, WANG Y J, LI S B, et al., 2020. Exhumation and landscape evolution in eastern South China since the Cretaceous: new insights from fission-track thermochronology[J]. *Journal of Asian Earth Sciences*, 191: 104239.
- WANG Y, ZUO R G, CAO K, et al., 2022. Late Mesozoic to Cenozoic exhumation of the SE South China Block: constraints from zircon and apatite fission-track thermochronology[J]. *Tectonophysics*, 838: 229518.
- XIE Y L, WU F L, FANG X M, 2019. Middle Eocene East Asian monsoon prevalence over southern China: evidence from palynological records[J]. *Global and Planetary Change*, 175: 13-26.
- XU C H, DENG Y L, BARNES C G, et al., 2023. Offshore-onshore tectono-magmatic correlations: towards a Late Mesozoic non-Andean-type

- Cathaysian continental margin [J]. *Earth-Science Reviews*, 240: 104382.
- XU X S, ZHAO K, HE Z Y, et al., 2021. Cretaceous volcanic-plutonic magmatism in SE China and a genetic model [J]. *Lithos*, 402-403: 105728.
- YAN L L, HE Z Y, JAHN B M, et al., 2016. Formation of the Yandangshan volcanic-plutonic complex (SE China) by melt extraction and crystal accumulation [J]. *Lithos*, 266-267: 287-308.
- YI Y, CARTER A, XIA B, et al., 2009. A fission-track and (U-Th)/He thermochronometric study of the northern margin of the South China Sea: an example of a complex passive margin [J]. *Tectonophysics*, 474(3-4): 584-594.
- YU M G, XING G F, SHEN J L, et al., 2006. Chronologic study on volcanic rocks in the Mt. Yandangshan world geopark [J]. *Acta Geologica Sinica*, 80(11): 1683-1690. (in Chinese with English abstract)
- YU Y W, XU B T, 1999. Stratigraphical sequence and geochronology of the upper Mesozoic volcano-sedimentary rock series in Zhejiang [J]. *Journal of Stratigraphy*, 23(2): 136-145. (in Chinese with English abstract)
- YUAN W M, MO X X, ZHANG A K, et al., 2013. Fission track thermochronology evidence for multiple periods of mineralization in the Wulonggou gold deposits, eastern Kunlun Mountains, Qinghai Province [J]. *Journal of Earth Science*, 24(4): 471-478.
- ZHANG F X, ZHANG D R, 1990. The circular features on the Xianju Landsat image and its volcanic structural significances [J]. *Journal of Zhejiang University (Natural Science)*, 24(3): 465-473. (in Chinese with English abstract)
- ZHANG J H, YANG J H, CHEN J Y, et al., 2018. Genesis of late early cretaceous high-silica rhyolites in eastern Zhejiang province, Southeast China: a crystal mush origin with mantle input [J]. *Lithos*, 296-299: 482-495.
- ZHANG R Y, YANG F L, HU P P, et al., 2021. Cenozoic tectonic inversion in the northern depression, South Yellow Sea basin, East Asia: structural styles and driving mechanism [J]. *Tectonophysics*, 798: 228687.
- ZHANG Y Q, DONG S W, LI J H, 2019. Late Paleogene sinistral strike-slip system along east Qinling and in southern North China: implications for interaction between collision-related block trans-rotation and subduction-related back-arc extension in East China [J]. *Tectonophysics*, 769: 228181.
- Zhejiang Provincial Geological Survey Institute, 2024. Regional geology of China, Zhejiang [M]. Beijing: Geological Press. (in Chinese)
- ZHENG Y F, XIAO W J, ZHAO G C, 2013. Introduction to tectonics of China [J]. *Gondwana Research*, 23(4): 1189-1206.
- ZHOU J, JIN C, SUO Y H, et al., 2021. Yanshanian mineralization and geo-dynamic evolution in the western Pacific Margin: a review of metal deposits of Zhejiang Province, China [J]. *Ore Geology Reviews*, 135: 104216.
- ZHOU J, JIN C, SUO Y H, et al., 2022. The Yanshanian (Mesozoic) metallogenesis in China linked to crust-mantle interaction in the western Pacific margin: an overview from the Zhejiang Province [J]. *Gondwana Research*, 102: 95-132.
- ZHOU L Y, HUANG L Y, HUANG J J, et al., 2013. Zhejiang geological tectonic environment and endogenous metallic deposits [J]. *Bulletin of Science and Technology*, 29(1): 25-33, 41. (in Chinese with English abstract)
- ZHOU X M, LI W X, 2000. Origin of Late Mesozoic igneous rocks in southeastern China: implications for lithosphere subduction and underplating of mafic magmas [J]. *Tectonophysics*, 326(3-4): 269-287.
- ZHOU X M, SUN T, SHEN W Z, et al., 2006. Petrogenesis of Mesozoic granitoids and volcanic rocks in South China: a response to tectonic evolution [J]. *Episodes*, 29(1): 26-33.
- ZHU W L, ZHONG K, FU X W, et al., 2019. The formation and evolution of the East China Sea Shelf Basin: a new view [J]. *Earth-Science Reviews*, 190: 89-111.

附中文参考文献

- 段文涛, 黄少鹏, 唐晓音, 等, 2017. 利用 ANSYS WORKBENCH 模拟火山岩浆活动热扩散过程 [J]. *岩石学报*, 33(1): 267-278.
- 段政, 赵希林, 邢光福, 等, 2015. 浙闽相邻区白垩纪上下火山岩系成因与壳幔作用对比研究 [J]. *地质学报*, 89(2): 319-338.
- 李三忠, 索艳慧, 刘博, 2018. 海底构造系统(上册) [M], 北京: 科学出版社.
- 李三忠, 曹现志, 王光增, 等, 2019. 太平洋板块中-新生代构造演化及板块重建 [J]. *地质力学学报*, 25(5): 642-677.
- 林旭, 吴中海, 董延钰, 等, 2024. 新生代亚洲季风的演化过程 [J]. *地质力学学报*, 30(4): 673-690.
- 阮宏宏, 陶奎元, 徐忠连, 1988. 括苍山地区火山构造 [J]. *中国地质科学院南京地质矿产研究所所刊*, 9(2): 81-94.
- 阮宏宏, 谢家莹, 陶奎元, 1993. 浙江括苍山巨型环形火山构造及其地质意义 [J]. *火山地质与矿产*, 14(4): 1-11.
- 水涛, 徐步台, 梁如华, 等, 1986. 绍兴-江山古陆对接带 [J]. *科学通报*, 31(6): 444-448.
- 水涛, 1987. 中国东南大陆基底构造格局 [J]. *中国科学*, 17(4): 414-422.
- 唐增才, 董学发, 孟祥随, 等, 2018. 浙江神仙居流纹质火山岩年代学、地球化学及其地质意义 [J]. *地层学杂志*, 42(2): 167-178.
- 陶奎元, 余明刚, 邢光福, 等, 2004. 雁荡山白垩纪破火山地质遗迹价值与全球对比 [J]. *资源调查与环境*, 25(4): 297-303.
- 王新毓, 索艳慧, 李三忠, 等, 2020. 华南东部陆缘新生代隆升历史及其动力学机制 [J]. *岩石学报*, 36(6): 1803-1820.
- 王学颖, 徐夕生, 赵凯, 2023. 浙东括苍山-雁荡山破火山白垩纪多旋回火山-侵入杂岩成因研究 [J]. *矿物岩石地球化学通报*, 42(5): 1062-1077.
- 谢家莹, & 徐忠连, 1988. 括苍山地区中生代火山旋回划分. *中国地质科学院南京地质矿产研究所所刊*, 9(02): 71-83.
- 余明刚, 邢光福, 沈加林, 等, 2006. 雁荡山世界地质公园火山岩年代学研究 [J]. *地质学报*, 80(11): 1683-1690.
- 俞云文, 徐步台, 1999. 浙江中生代晚期火山-沉积岩系层序和时代 [J]. *地层学杂志*, 23(2): 136-145.
- 张福祥, 张登荣, 1990. 仙居幅卫片上环形体的火山构造意义 [J]. *浙江大学学报(自然科学版)*, 24(3): 465-473.
- 浙江省地质调查院, 2024. 中国区域地质志·浙江志 [M]. 北京: 地质出版社.
- 周乐尧, 黄立勇, 黄建军, 等, 2013. 浙江地质构造环境与内生金属矿床成矿初探 [J]. *科技通报*, 29(1): 25-33, 41.